Chinese Chemical Letters 33 (2022) 3113–3118

Contents lists available at ScienceDirect

Chinese Chemical Letters

journal homepage: www.elsevier.com/locate/cclet

Mg-induced g-C_3N_4 synthesis of nitrogen-doped graphitic carbon for effective activation of peroxymonosulfate to degrade organic contaminants

Jihong Xu[a], Jianxin Song[a], Yulin Min[a,b], Qunjie Xu[a,b], Penghui Shi[a,b,*]

[a] Shanghai Key Laboratory of Materials Protection and Advanced Materials in Electric Power, Shanghai University of Electric Power, Shanghai 200090, China
[b] Shanghai Institute of Pollution Control and Ecological Security, Shanghai 200090, China

ARTICLE INFO

Article history:
Received 5 August 2021
Revised 5 September 2021
Accepted 4 October 2021
Available online 10 October 2021

Keywords:
Mg-induced
Graphene
PMS activation
Nonradical process
Bisphenol A
Toxicity

ABSTRACT

The nitrogen-doped carbon derived from graphitic carbon nitride (g-C_3N_4) has been widely deployed in activating peroxymonosulfate (PMS) to remove organic pollutants. However, the instability of g-C_3N_4 at high temperature brings challenges to the preparation of materials. The nitrogen-doped graphitic carbon nanosheets (N-GC750) were synthesized by magnesium thermal denitrification. Magnesium undergoes the displacement reaction with small molecules produced by the pyrolysis of g-C_3N_4, thereby effectively fixing carbon on the *in-situ* template of Mg_3N_2 and avoiding direct product volatilization. N-GC750 exhibited excellent performance during the PMS activation process and bisphenol A (BPA, 0.2 g/L) could be thoroughly removed in 30 min. A wide range of pH (3–11), temperature (10–40 °C) and common anions were employed in studying the impact on system. Additionally, N-GC750 showed satisfactory reusability in cycle tests and promising applicability in real water samples. Quenching experiments and electron paramagnetic resonance (EPR) measurements indicated that singlet oxygen was the main active species coupled with partial electron transfer in N-GC750/PMS system. Furtherly, the oxidation products were identified, and their ecotoxicity was evaluated. This work is expected to provide a reference for the feasibility of preparing g-C_3N_4 derived carbon materials and meaningful for PMS activation.

Selective removal of emerging organic contaminants (EOCs) from the environment has been the research focus because of their low concentration, difficult degradation, and high ecological risk in recent years [1–3]. Efficient removal of EOCs is essential for drinking water safety and ecological protection. Advanced oxidation processes based on nonradical (*e.g.*, surface activated peroxodisulfate/peroxymonosulfate [4], electron transfer [5], singlet oxygen [6], high-valent metals [7], inorganic oxidants [8]) can effectively remove EOCs. It can be attributed to high adaptability in a wide pH range and could not be affected by various ions and background natural organic matter [9]. Meanwhile, it has a moderate redox potential and good selectivity to target pollutants [10]. Carbon materials, whose catalytic performance is proven to surpass many transition metals and their oxides, can effectively activate PMS to rapidly remove organic pollutants in the form of nonradicals [11–13].

Graphene is a carbon material with single or multiple carbon layers and sp^2 (trigonal) hybrid carbon lattice [14] and is proven to be excellent catalytic material. For example, Duan *et al.* [15] found that reduced graphene oxide can effectively activate PMS to generate sulfate radicals to degrade organic pollutants. It is worth noting that the natural graphite reserves are limited, whereas its demand is increasing. The traditional method of preparing graphite (Acheson [16] process) relies on amorphous carbon as the precursor to synthesize graphite at 3000 °C, consuming high energy and depending on equipment. Therefore, synthesizing graphite method with low energy consumption, high output, and simple process is important. The ability of pure graphene to activate PMS is limited, and a series of heterogeneous element doping processes have been developed, including boron doping [17], sulfur doping [18], nitrogen doping [15,19]. Among which nitrogen doping attracted much attention because it could well adjust the chemical properties of the carbon material surface and the electron distribution in the carbon skeleton and bring more active sites [20,21].

Graphite carbon nitride (g-C_3N_4) as a precursor for the synthesis of nitrogen-doped carbon has received extensive attention [22]. With the unique conjugated structure and high nitrogen content,

* Corresponding author at: Shanghai Institute of Pollution Control and Ecological Security, Shanghai 200090, China.
E-mail address: shipenghui@shiep.edu.cn (P. Shi).

https://doi.org/10.1016/j.cclet.2021.10.005
1001-8417/

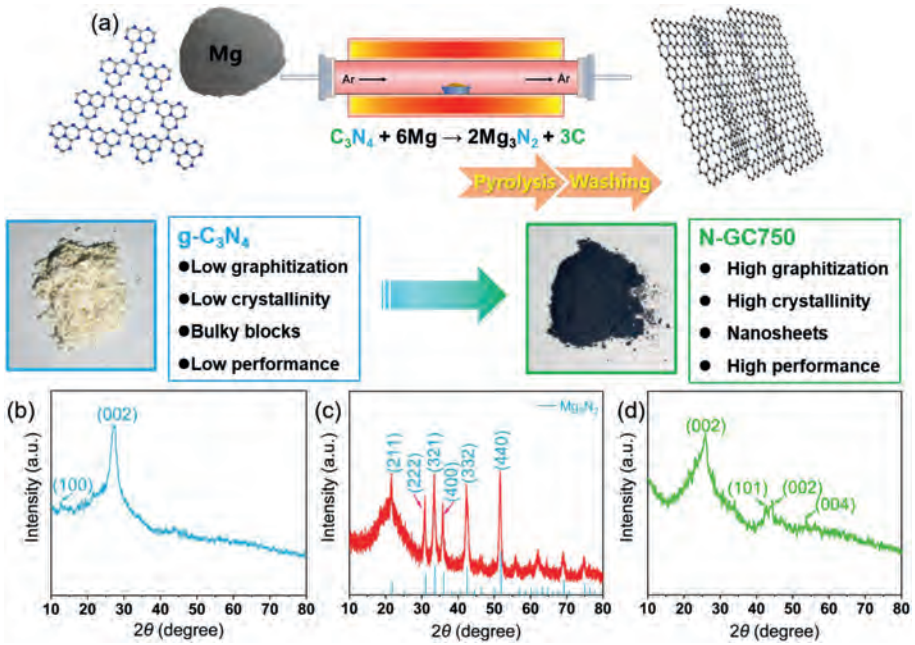

Fig. 1. (a) Schematic illustration of material synthesis process. (b–d) XRD pattens of g-C_3N_4 precursor, mixtures after pyrolysis, and N-GC750, respectively.

g-C_3N_4 is often used as a self-sacrificial template synthetic material. However, given that g-C_3N_4 decomposes and volatilizes at high temperatures (> 750 °C) to form gaseous substances, it is difficult to generate target materials, while graphitized carbon materials generally require higher temperatures (900 °C) [22]. Furthermore, the instability of nitrogen at high temperatures makes g-C_3N_4 lose a large amount of nitrogen during the heating process [14], providing large space to synthesize nitrogen-doped graphene with g-C_3N_4 at a lower temperature.

In this work, a simple and effective method was verified to convert low-cost g-C_3N_4 into nitrogen-doped graphite carbon nanosheets through the magnesium thermal denitrification process. The resulting graphene exhibited excellent catalytic activity for the degradation of bisphenol A (BPA) during the PMS activation process, better than commercial carbon catalysts (carbon nanotubes (CNT), reduced graphene oxide (RGO)) and common transition metal catalysts (Co_3O_4, MnO_2, Fe_3O_4). Quenching experiments and electron paramagnetic resonance (EPR) measurements proved that singlet oxygen played a leading role in BPA degradation. Furthermore, the electron transfers also contributed to BPA removal. The anti-interference ability of nitrogen-doped graphitic carbon nanosheets (N-GC750)/PMS in a complex water matrix and the actual water phase was conducted. Significantly, the ecotoxicity assessment of oxidation products and the applicability of the N-GC750/PMS system were evaluated.

Materials and methods are listed in supporting information. An X-ray diffractometer (XRD) was used to prove the possibility of g-C_3N_4 conversion to graphene. Fig. S1 (Supporting information) presents standard XRD patterns of g-C_3N_4, Mg_3N_2, and graphite [23,24]. As shown in Fig. 1, the XRD pattern of the g-C_3N_4 precursor showed two obvious peaks at $2\theta = 13.05°$ and $2\theta = 27.62°$, attributing to typical 100 and 002 planes of g-C_3N_4 [25]. It was a pale-yellow solid powder from the appearance. However, after adding magnesium powder for calcination, a black carbon material was found in the light-yellow g-C_3N_4 powder, indicating that the original g-C_3N_4 structure was rearranged under the conditions of the magnesium thermal denitrification reaction. The XRD pattern showed that the products of the pyrolysis reaction of magnesium powder and g-C_3N_4 are mainly carbon and magnesium nitride. Therefore, magnesium can fix carbon on the *in-situ* template magnesium nitride under high temperature, reducing the direct volatilization of carbon. After being pickled, the XRD patterns of the product showed obvious peaks at $2\theta = 26.1°$, 42.8°, 44.3°, 56.3°, which were usually attributed to 002, 101 and 004 crystal planes [14,26]. Therefore, N-GC750 had a high graphitization degree and crystallinity than the g-C_3N_4 precursor.

To evaluate the morphological and structural characteristics of the catalyst, as well as the role of magnesium powder to graphite carbon materials in the conversion of g-C_3N_4 precursors, scanning electron microscopy (SEM) and transmission electron microscopy (TEM) on the N-GC750 were performed. Fig. S2a (Supporting information) showed an SEM image of the typical graphite phase carbon nitride. It can be observed that the g-C_3N_4 obtained by urea air calcination had no sintering agglomeration, and had a very thin layer structure, which provided a precursor material for the synthesis of high-quality graphene material. Fig. S2b (Supporting information) showed the morphology of N-GC750 collected after calcination of g-C_3N_4 and magnesium powder at high temperature, and the phenomenon of lamella fracture could be observed. N-GC750 presented a three-dimensional petal-like shape. This structure has a higher specific surface area and provides more active sites than ordinary spherical particles, which is beneficial to the progress of catalytic reactions [22,27,28].

The TEM images of N-GC750 (Figs. S2c and d in Supporting information) confirmed the laminar structure of the material again. In the high-resolution HRTEM image, lattice fringes were showed clearly with the lattice spacing in 0.34 nm measured by the digital software. The high crystallinity of N-GC750 was also confirmed by its electron diffraction pattern (Fig. S3 in Supporting information). The thin sheets and ordered morphology of the N-GC750 might facilitate electron transfer and provide abundant active sites [29,30]. As illustrated in Fig. S2e (Supporting information), the uniform distribution of the nitrogen parts in the graphene carbon matrix provided convenience for PMS activation.

Raman spectroscopy was further used to explore the structural changes of g-C_3N_4 after high-temperature magnesium thermal denitrification treatment (Fig. S4a in Supporting information). There was no significant Raman signal for g-C_3N_4 owing to the

strong fluorescence effect [25]. In contrast, the N-GC750 was like the graphene-based material. The D band and G band of carbon materials are concerned with structure defect and graphitization [31,32]. Two apparent peaks in the D band (1363 cm^{-1}) and G band (1572 cm^{-1}) further confirmed the conversion of g-C_3N_4 to three-dimensional graphene after magnesium thermal reaction. The high-intensity D band indicated the defects existed in N-GC750, possibly caused by nitrogen-doped into the carbon substrate. Successful doped of nitrogen could adjust the electronic structure of the surrounding carbon, and promote PMS activation [33].

N_2 adsorption-desorption analysis of g-C_3N_4 and N-GC750 was carried out to unveil their specific surface area and porosity (Fig. S4b in Supporting information). G-C_3N_4 and N-GC750 showed a typical hysteresis loop, type IV isotherms (a typical mesoporous structure). After the magnesium thermal denitrification process, the specific surface area of N-GC750 (227.4 m^2/g) was three times higher than the pristine g-C_3N_4 (71.2 m^2/g) (Table S3 in Supporting information). Additionally, the pore size distribution determined by the Barret-Joyner-Halenda (BJH) method reflects that the pores of g-C_3N_4 were mainly distributed in a range of 0–10 nm, which was in agreement with previous reports [34]. Compared with g-C_3N_4, N-GC750 increased its mesopore volume in the 0.4–1.0 pressure range because of the merged mesoporous. It manifests that the surface area and pore volume could be improved in nitrogen removal, which was beneficial to activate PMS. A large specific surface area allows the catalyst to expose more active sites, and increases the contact between the catalyst and compound. The mesoporous structure facilitates the adsorption of pollutants on the catalyst surface and accelerates the mass transfer process [12,35].

X-ray photoelectron spectroscopy (XPS) was used to detect and clarify the conversion of the g-C_3N_4 precursor to the chemical composition of N-GC750. Fig. S4c and Table S4 (Supporting information) showed the XPS total spectrum of the two and the content of the corresponding elements. The g-C_3N_4 precursor had a higher nitrogen content (63%) and a lower carbon content (35%). After the magnesium thermal denitrification process, N-GC750 presented a high carbonization degree with high 94.73% carbon content, which undoubtedly proved that magnesium played a good role in carbon fixation. According to the high-resolution XPS results (Figs. S4d, S5 and S6 in Supporting information), the C 1s spectra of g-C_3N_4 showed that two deconvoluted peaks, respectively, correspond to N–C=N and C=C [24]. The N-GC750 shows that C=C is the main component, and N–C=N has shifted. Furthermore, the N 1s spectra of g-C_3N_4 show that two deconvoluted peaks, respectively, correspond to pyridinic N (398.69 eV) and graphitic N (400.48 eV) [25]. But the residual nitrogen of N-GC750 existed mainly in the pyridine nitrogen form. XPS further proves that g-C_3N_4 has been transformed into nitrogen-doped graphene. Introducing pyridine nitrogen can be an active site and improve catalytic activity. Pyridine nitrogen is generally recognized as a Lewis acid-base, used as an adsorption site for PMS and phenolic compounds to promote redox reactions [15,36]. Therefore, the residual pyridine nitrogen in N-GC750 may contribute to its catalytic ability greatly.

The catalytic performance of N-GC750 was assessed with BPA. In Fig. 2a, the PMS additive alone displayed a negligible effect on BPA degradation. The BPA removal rate could reach 8% while g-C_3N_4 and PMS coexist in the system, indicating that g-C_3N_4 had certain abilities to catalyze PMS. Surprisingly, when N-GC750 was used as the catalyst for activating PMS, the BPA concentration was completely degraded and reached a mineralization rate of 55% (Fig. S7 in Supporting information) in 30 min, showing excellent ability to activate PMS. Fig. S8 (Supporting information) exhibits a good linear relationship between BPA degradation with time in N-GC750/PMS system. The pseudo-first order kinetic model is applied to interpret the kinetic data [37,38]. This is possibly attributed to forming the N-doped three-dimensional graphene structure, which provides new active sites for PMS [12,22]. Carbon materials usually have a large adsorption capacity to affect the removal efficiency of organics. The adsorption capacity of N-GC-750 and g-C_3N_4 on BPA were evaluated. The small pore structure and specific surface area of g-C_3N_4 determined that about 2% of BPA was removed in 30 min. After high-temperature magnesium thermal denitrification, 8% BPA was adsorbed by N-GC750 because of its increased specific surface area and new adsorption sites. In addition, the catalytic performance of materials prepared at different temperatures was explored (Fig. S9 in Supporting information). Considering the cost of process and the properties of materials comprehensively, N-GC750 was selected for further research.

To further evaluate the catalytic performance of N-GC750 on PMS activation, common commercial carbon catalysts (CNT, RGO) and transition metal oxides (Co_3O_4, MnO_2, Fe_3O_4) were selected. As shown in Fig. 2b, N-GC750 exhibits excellent performance within 30 min, whose ability to catalyze and oxidize BPA was 2.2 times that of CNT, three times that of Co_3O_4, and six times that of Fe_3O_4.

To assess the applicability of N-GC750, pH value, reaction temperature, inorganic ions, and the number of cycles were selected as single variables to explore the impact on the N-GC750/PMS system. The pH value often limits the oxidation ability of active species in the advanced oxidation process. For example, the hydroxyl radicals produced by the Fenton reaction perform best under acidic conditions, while sulfate radicals are more suitable for neutral environments [39]. Fig. 2c shows the BPA removal rate by N-GC750/PMS at different pH values. In the range of pH 3–9, the high BPA removal efficiency was observed in the N-GC750/PMS system. When the pH continues to rise, the degradation efficiency was significantly reduced. This can be explained by the surface charge of N-GC750 (Fig. S10 in Supporting information). N-GC750 is positively charged under acidic conditions, indicating the protonation of nitrogen and carbon atoms. When N-GC750 is under alkaline conditions, the surface of N-GC750 will electrostatically repel BPA and PMS, which will cause the performance of N-GC750 to deteriorate under alkaline conditions [22]. The result is superior to the traditional free radical reaction (reaction dominated by hydroxyl radicals or sulfate radicals), indicating that the new reactive oxygen species (ROS) produced in the reaction system can oxidize BPA, and has a wider range of pH value (3–9) adaptation.

Temperature is also an essential factor affecting the degradation efficiency of pollutants. In this study, the catalytic oxidation reaction temperature was controlled by a constant temperature oscillating reactor, to assess its effects on the BPA degradation in the N-GC750/PMS system. The reaction temperature was directly proportional to the degradation efficiency of BPA in Fig. 2d. The BPA degradation efficiency gets higher as the temperature increases. When the temperature was 10 °C, the degradation rate of BPA was 97% within 30 min, but a small amount of BPA was still not degraded. When the temperature rose to 25 °C, BPA was utterly degraded within half an hour. When the reaction temperature was further increased to 40 °C, BPA was completely degraded in 20 min. According to the Arrhenius equation, the activation energy (E_a) of N-GC750 was 29.28 kJ/mol, which is lower than nitrogen-doped graphene (31.6 kJ/mol) [40] and nitrogen-doped carbon nanotubes (36.0 kJ/mol) [41]. The low activation energy may be the reason for the high efficiency of N-GC750/PMS system. Therefore, temperature increasing accelerates the activation of the PMS molecules by the catalyst to produce more oxygen-active substances. On the other hand, high temperature provides more energy to activate BPA molecules, thereby reducing the activation energy required for degradation reactions.

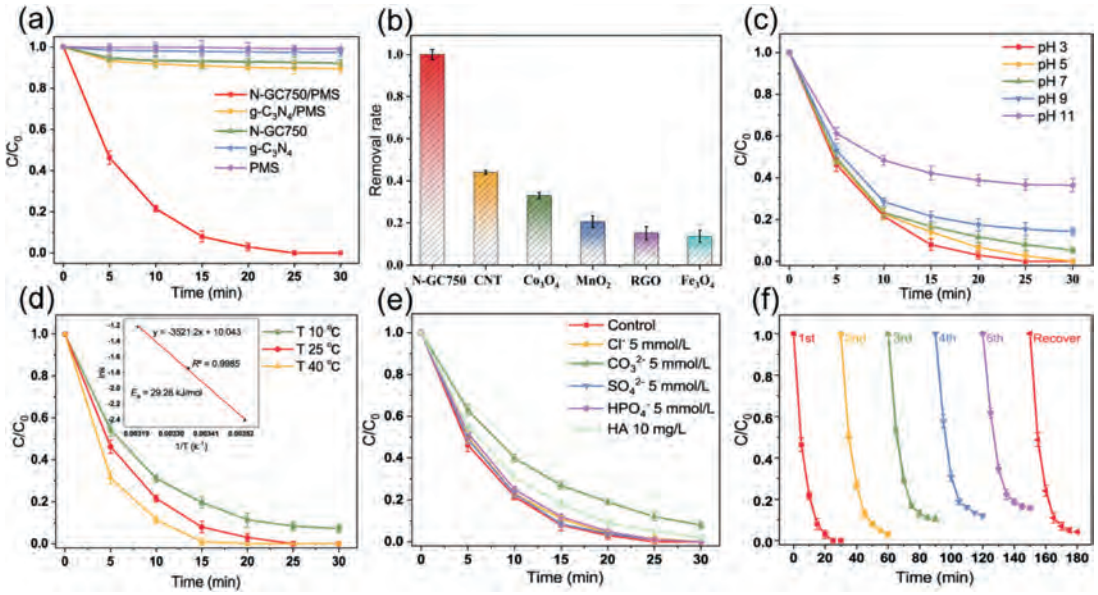

Fig. 2. (a, b) Degradation of BPA in different systems, the effects of (c) initial pH, (d) temperature, (e) inorganic anions on BPA degradation in N-GC750/PMS system, (f) the property of recycled N-GC750 for the degradation of BPA ([PMS] = 0.2 g/L, [catalyst] = 0.1 g/L, [BPA] = 0.2 g/L).

In the free radical oxidation reaction, free radicals are often interfered with and inactivated by inorganic anions in water. For example, hydroxyl radical is consumed to react with Cl^- in water, thereby affecting the degradation rate of pollutants [42]. In this study, several common inorganic anions (Cl^-, CO_3^{2-}, SO_4^{2-}, HPO_4^-, humic acid (HA)) were used as interfering ions to explore their influence on the reaction. BPA being completely degraded in 30 min in the presence of SO_4^{2-}, Cl^-, and HPO_4^- (Fig. 2e). CO_3^{2-} and HA slightly affected the removal of BPA. This may be the competition of BPA with CO_3^{2-} or HA for ROS [6,43]. Results showed that N-GC750 had a strong anti-interference ability to inorganic anions, which further proved that the N-GC750/PMS system oxidation of BPA was a nonradical oxidation process.

The N-GC750/PMS system was also evaluated to remove BPA from actual water bodies. Surface water (SW) and sewage treatment plant effluent (ST) are selected as actual wastewater, with related wastewater composition shown in Fig. S11 (Supporting information) and Table S5 (Supporting information). As shown in Fig. S12 (Supporting information), the removal rate of BPA in SW and ST was slightly limited with BPA removed within 30 min, which proved that N-GC750 was less interfered by background water matrix in the presence of PMS.

The cycle stability of the catalyst is an important reference factor for evaluating the overall catalyst performance. The used catalysts were washed, dried and recovered. Cyclic degradation experiments were conducted to evaluate their cyclic stability. Results showed that the catalyst basically maintained its original performance in the first cycle, but slightly decreased in the following cycles. After four cycles, the degradation capacity of the system to BPA was 89% (Fig. 2f). The reason was that the reaction intermediates produced during the catalysis process could not fall off quickly, resulting in the occupation of the active sites of the chemical reaction. When the catalyst was annealed at a high temperature to restore its active sites, the catalyst performance rebounded, which confirmed the conjecture.

The selective degradation of different organics in the N-GC750/PMS system was also studied. Nitrobenzene (NB) is often used as a chemical probe for $^{\bullet}OH$ (k_2(NB, $^{\bullet}OH$) = 3.9×10^9 L mol^{-1} s^{-1}), and benzoic acid (BA) is used as a chemical probe for $SO_4^{\bullet-}$ (k_2(BA, $SO_4^{\bullet-}$) = 1.2×10^9 L mol^{-1} s^{-1}) and $^{\bullet}OH$ (k_2 (BA, $^{\bullet}OH$) = 4.2×10^9 L mol^{-1} s^{-1}) [6]. As shown in Fig. S13 (Supporting information), BA and NB had little effect in the N-GC750/PMS system, which proved that free radicals ($^{\bullet}OH$, $SO_4^{\bullet-}$) were not generated in the system again. The ionization potentials (IP) value of organic pollutants has become an important indicator for evaluating oxidation and price reduction [44]. The oxidation ability of the N-GC750/PMS system to these pollutants can be roughly divided into three levels. NB and BA had a higher IP value, showed oxidation resistance to the system, and *p*-hydroxybenzoic acid (HBA) with a medium IP value had a mild removal efficiency (51%). Phenol (PN) with a lower IP value was degraded by 95% in 30 min, Rhodamine B (RHB) and BPA were completely oxidized in 30 min. This result showed the N-GC750/PMS system was different from the previously reported free radical oxidation system (free radicals oxidize pollutants indifferently). The selective oxidation experiment of the N-GC750/PMS system further proved that the removal of organic matter does not depend on free radical reactions.

PMS can be activated through many ways to produce active species to degrade organic pollutants. In order to clarify the catalytic mechanism in the N-GC750/PMS system, quenching experiments were performed to use methanol and *tert*–butanol as free radical scavengers due to their high reactivity to sulfate radicals (k(MeOH, $SO_4^{\bullet-}$) = 1.67×10^7 to 7.7×10^7 L mol^{-1} s^{-1}) and hydroxyl radicals (k(MeOH, $^{\bullet}OH$) = 9.7×10^8 L mol^{-1} s^{-1}, k(TBA, $^{\bullet}OH$) = 3.8×10^8 to 7.6×10^8 L mol^{-1} s^{-1}) [6,45]. As shown in Fig. 3a, the addition of methanol and *tert*-butanol had little effect on removing BPA, indicating that BPA removal may not depend on the free radicals in the N-GC750/PMS system.

It was reported that nitrogen-doped carbon can activate PMS to generate singlet oxygen and remove pollutants [8,11]. Sodium azide was an effective scavenger for singlet oxygen ($k = 2.5 \times 10^9$ L mol^{-1} s^{-1}) in quenching experiments [34]. Results showed that the BPA removal efficiency was significantly slowed down in the presence of sodium azide (Fig. 3a), which proved that singlet oxygen may play an important role in BPA removal. 2,2,6,6-tetramethyl-4-piperidinol (TEMP) was used as a spin trap and EPR was used to detect the presence of singlet oxygen. Fig. 3b shows an obvious characteristic triple signal (1:1:1) in the N-GC750/PMS system, attributed to the presence of singlet oxygen [32]. In addition, although a certain singlet oxygen signal was observed in the

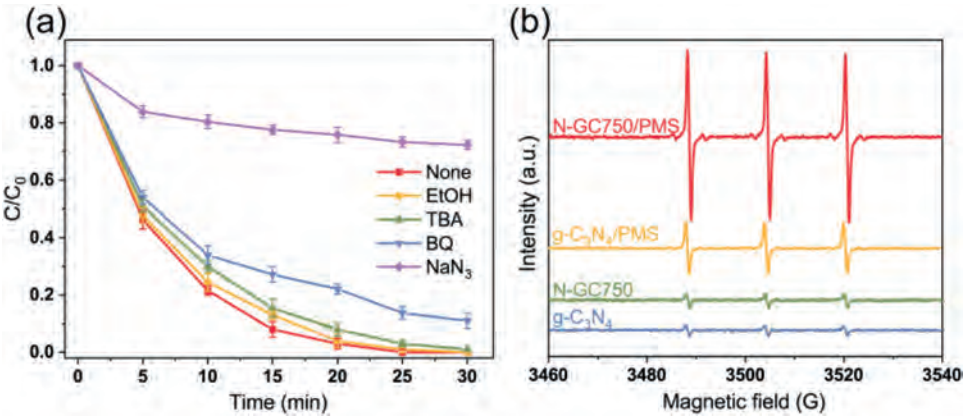

Fig. 3. (a) Inhibition effect of different quenchers on BPA degradation in N-GC750/PMS system ([TBA] = 1 mol/L, [MeOH] = 1 mol/L, [BQ] = 10 mmol/L, [NaN_3] = 20 mmol/L, [PMS] = 0.2 g/L, [catalyst] = 0.1 g/L, [BPA] = 0.2 g/L), (b) EPR spectrum of TEMP-$^1O_2$. ([PMS] = 0.2 mmol/L, [catalyst] = 0.1 g/L, [BPA] = 0.2 g/L, [TEMP] = 0.35 mol/L).

g-C_3N_4/PMS system, it was weaker than that of the N-GC750/PMS system. This was consistent with the results of BPA degradation (Fig. 2a), which further proved the advantages of converting g-C_3N_4 into carbon materials.

Superoxide radicals are often recombined with water to produce singlet oxygen in the activated PMS system of carbon materials [46,47]. As a scavenger of superoxide radicals, *p*-benzoquinone (BQ) is used to determine the contribution of superoxide radicals to BPA removal (Fig. 3a). BPA removal was inhibited to a certain extent after the BQ additive. 5,5-Dimethyl-1-pyrroline N-oxide (DMPO) was used as the trapping agent in the methanol system. EPR was used to measure the superoxide radicals, the superoxide signal generated by pure N-GC750 can be ignored (Fig. S14 in Supporting information). However, the N-GC750/PMS formed the signal of superoxide radicals ware significantly enhanced. Therefore, it is determined that superoxide radicals are generated in the N-GC750/PMS system and participate in removing BPA.

In recent studies, it has been observed that a lower nitrogen content in carbon improves the oxidation–reduction reaction (ORR) performance [48]. In addition, the partial loss of nitrogen atoms will induce defects in the adjacent carbon, thereby enhancing the performance of carbon materials [32]. Meanwhile, the higher specific surface area and porous structure are beneficial to the adsorption of pollutants on the surface of carbon materials and promote the degradation [35]. In this work, the substitution reaction between g-C_3N_4 and magnesium powder resulted in a large amount of nitrogen removal (Fig. S4c and Table S4). The XPS measurements showed that the remaining 2.75% nitrogen was pyridine nitrogen (Fig. S4d). As mentioned above, pyridine nitrogen is generally considered to be a Lewis acid-base, used as an adsorption site for PMS and phenolic compounds to promote redox reactions. Furthermore, the presence of residual nitrogen provides a high electron density, which can attract more electrons from adjacent carbon atoms, resulting in a decrease in the electron density of carbon atoms [49]. This provided a site for the activation of PMS and led to the generation of ROS.

It was worth noting that although various quenchers achieved different effects in the G-GC750/PMS system, none of them terminated the reaction completely. Electrochemical techniques were used to explore other possible mechanisms. As shown in Fig. S15 (Supporting information), the open-circuit potential of the glassy carbon electrode coated with N-GC750 increased significantly with the PMS additive. In contrast, the potential decreases greatly after the BPA additive continuously. The potential of the pure glassy carbon electrode did not change significantly. Therefore, it was probably that a significant electron transfer process occurred in the N-GC750/PMS system. Numerous studies have shown that carbon materials with defects are the active center for activating PMS to form nonradicals [5,32]. Raman spectroscopy (Fig. S4a) proved that defects or vacancies were formed due to the thermal denitrification of magnesium. Usually, the defective part has higher activity and shows completely different chemical and electronic characteristics [25]. Defects also play an important role in pollution adsorption [31]. The strong interaction between defect sites and pollutants allows PMS molecules to directly oxidize pollutants by extracting electrons from the adsorbed organic matter without generating free radicals. Therefore, parts of the BPA degradation were directly oxidized due to electron transfer caused by defects.

To verify the eco-environmental friendliness of N-GC750/PMS system, GC–MS was used to determine the BPA product in the N-GC750/PMS system. Fig. S16 and Table S6 (Supporting information) listed possible degradation intermediates. ECOSAR program in QSAR was used to predict the ecotoxicities of target pollutants and their intermediate products [4,50–52]. As shown in Table 1, Figs. S17 and S18 (Supporting information), the toxicity of BPA ranged from toxic (1 mg/L < lethal concentration (LC_{50})/effect concentration (EC_{50})/chronic value (ChV) ≤ 10 mg/L) to very toxic (LC_{50}/EC_{50}/ChV ≤ 1 mg/L), very close to the toxicity of the parent pollutant (m/z = 164.24, 340.42, 254.32, 192.25) compared with the toxicity of the product formed by the initial reaction. Generally, the toxicity of the products in the system decreased gradually. Compared with the parent BPA, the acute toxicity of the transformed products (*e.g.*, m/z = 286.32, 110.11) was not harmful to fish, and the LC_{50} values for daphnid were even two orders of magnitude higher. Chronic toxicity was continuously reduced in target pollutants. The value of chronic toxicity increased by one order of magnitude, especially for fish, and two orders of magnitude for daphnid reduced the chronic toxicity of m/z = 110.11. Open ring structures and small molecules of acids (m/z = 147, 87, 74, 60) were also identified in GC–MS, whose acute toxicity was nontoxic or harmless, with no harm to fish, daphnid, and green algae. Therefore, further degradation of the initial products generated less harmful products. Acute toxicity of the BPA could be significantly reduced after the N-GC750/PMS treatment, and N-GC750/PMS oxidation was a promising strategy to degrade BPA and eliminate toxicity

In this research, magnesium underwent a substitution reaction with small g-C_3N_4 molecules produced by pyrolysis of g-C_3N_4 to construct porous nitrogen-doped carbon nanosheets. In the presence of PMS, it can effectively remove organic pollutants. The porous structure and the remaining pyridine nitrogen may play a central role in the catalytic process. Quenching experiments, EPR spectroscopy and electrochemical analysis show that singlet oxygen is the main active substance, and the mediation electron trans-

Table 1.
Estimated acute and chronic toxicity for fish, daphnid and green algae of BPA and their products by ECOSAR.

Compound (*m/z*)	Acute toxicity [a]			Chronic toxicity [a]		
	Fish (LC_{50}[b])	Daphnid (LC_{50}[b])	Green algae (EC_{50}[c])	Fish (ChV[d])	Daphnid (ChV[d])	Green algae (ChV[d])
228 (BPA)	1.28	5.24	1.33	0.55	1.77	0.227
164.24	1.08	1.11	0.102	0.13	0.17	0.343
340.42	1.08	1.67	0.459	0.045	0.515	0.290
254.32	9.26	5.98	7.54	1.05	0.831	2.62
192.25	12.5	7.93	9.44	1.39	1.06	3.18
286.32	22.8	103	20.4	10.2	35.4	3.34
110.11	22.2	256	4.9	14.2	101	0.568
87	141	78.1	52.9	13.4	7.15	13.2
147	255	140	90.8	24	12.4	22.1
74	1.15×10^4	5.74×10^3	2.48×10^3	965	388	485
60	2.58×10^4	1.23×10^4	4.40×10^3	2.05×10^3	732	778

[a] mg/L.
[b] LC_{50}: Median lethal concentration. A statistically derived concentration of a substance that can be expected to cause death in 50% of test animals.
[c] EC_{50}: Median effect concentration. A statistically derived concentration of a substance that can be expected to cause a specific effect (*e.g.*, growth inhibition) in 50% of test animals.
[d] ChV is defined as the geometric mean of the no observed effect concentration and the lowest observed effect concentration.

fer also contributed. Further research is found that N-GC750 has strong adaptability to inorganic anions and pH in water, showing excellent catalytic effects in real water samples. The ecotoxicity of identified products under the N-GC750 system is significantly reduced compared with the parent compound. In general, this research proved the possibility of easy conversion of g-C_3N_4 into graphite. Given its excellent performance in the PMS activation process, N-GC750 has a good prospect in actual wastewater treatment.

Declaration of competing interest

The authors declare that they have no known competing financial interests or personal relationships that could have appeared to influence the work reported in this paper.

Acknowledgments

The study was supported by the Science and Technology Commission of Shanghai Municipality (Nos. 21ZR1425200, 18020500800, 18JC1412900 and 19DZ2271100).

Supplementary materials

Supplementary material associated with this article can be found, in the online version, at doi:10.1016/j.cclet.2021.10.005.

References

[1] R.P. Schwarzenbach, B.I. Escher, K. Fenner, et al., Science 313 (2006) 1072–1077.
[2] S. Schulze, D. Zahn, R. Montes, et al., Water Res. 153 (2019) 80–90.
[3] K. Qian, H. Chen, W. Li, et al., Environ. Sci. Technol. 55 (2021) 7034–7043.
[4] Y. Qian, J. Huang, X. Liu, et al., Water Res. 185 (2020) 116278.
[5] P. Shao, S. Yu, X. Duan, et al., Environ. Sci. Technol. 54 (2020) 8464–8472.
[6] S. Zhu, X. Li, J. Kang, X. Duan, S. Wang, Environ. Sci. Technol. 53 (2019) 307–315.
[7] H. Li, C. Shan, B. Pan, Environ. Sci. Technol. 52 (2018) 2197–2205.
[8] Y. Ding, X. Wang, L. Fu, et al., Sci. Total Environ. 765 (2021) 142794.
[9] M.M. Mian, G.J. Liu, Chem. Eng. J. 392 (2020) 123681.
[10] S. Luo, Z.S. Wei, D.D. Dionysiou, et al., Chem. Eng. J. 327 (2017) 1056–1065.
[11] X. Duan, H. Sun, S. Wang, Acc. Chem. Res. 51 (2018) 678–687.
[12] S. Zhu, X. Huang, F. Ma, et al., Environ. Sci. Technol. 52 (2018) 8649–8658.
[13] K. Luo, Q. Yang, Y. Pang, et al., Chem. Eng. J. 374 (2019) 520–530.
[14] Y. Yuan, T. Wang, H. Chen, et al., Angew. Chem. Int. Ed. 59 (2020) 21935–21939.
[15] X. Duan, H. Sun, Y. Wang, J. Kang, S. Wang, ACS Catal. 5 (2014) 553–559.
[16] X. Jin, R. He, S. Dai, Chemistry 23 (2017) 11455–11459.
[17] H. Sun, Y. Wang, S. Liu, et al., Chem. Commun. 49 (2013) 9914–9916.
[18] X. Duan, K. O'Donnell, H. Sun, Y. Wang, S. Wang, Small 11 (2015) 3036–3044.
[19] L. Xu, C.X. Wu, P.H. Liu, et al., Chem. Eng. J. 387 (2020) 124065.
[20] J. Yu, L. Tang, Y. Pang, et al., Chem. Eng. J. 364 (2019) 146–159.
[21] W. Ren, G. Nie, P. Zhou, et al., Environ. Sci. Technol. 54 (2020) 6438–6447.
[22] J. Miao, W. Geng, P.J.J. Alvarez, M. Long, Environ. Sci. Technol. 54 (2020) 8473–8481.
[23] H. Ji, P. Du, D. Zhao, et al., Appl. Catal. B: Environ. 263 (2020) 118357.
[24] Y. Ding, C. Yu, J. Chang, et al., Small 16 (2020) e1907164.
[25] J. Liu, Y. Zhang, L. Zhang, et al., Adv. Mater. 31 (2019) e1901261.
[26] J. Peng, N. Chen, R. He, et al., Angew. Chem. Int. Ed. 56 (2017) 1751–1755.
[27] A. Vinu, Adv. Funct. Mater. 18 (2008) 816–827.
[28] Y. Chen, X.W. Dou, M.M. Zhang, et al., Chin. Chem. Lett. 26 (2015) 1144–1146.
[29] C. Tan, X. Cao, X.J. Wu, et al., Chem. Rev. 117 (2017) 6225–6331.
[30] J. Chen, Z. Mao, L. Zhang, et al., ACS Nano 11 (2017) 12650–12657.
[31] K. Lu, Z. Min, J. Qin, et al., Sci. Total. Environ. 752 (2021) 142282.
[32] J. Wang, X. Duan, J. Gao, et al., Water Res. 185 (2020) 116244.
[33] W. Ren, G. Nie, P. Zhou, et al., Environ. Sci. Technol. 54 (2020) 6438–6447.
[34] J. Qin, L. Dai, P. Shi, et al., J. Hazard. Mater. 398 (2020) 122808.
[35] X. Wang, Y. Qin, L. Zhu, H. Tang, Environ. Sci. Technol. 49 (2015) 6855–6864.
[36] Y. Wang, N. Ren, J. Xi, et al., ACS ES&T Eng. 1 (2021) 32–45.
[37] Y. Liu, L. Chen, X. Liu, et al., Chin. Chem. Lett. 33 (2022) 1385–1389.
[38] M. Ma, L. Chen, J. Zhao, W. Liu, H. Ji, Chin. Chem. Lett. 30 (2019) 2191–2195.
[39] J. Lee, U. von Gunten, J.H. Kim, Environ. Sci. Technol. 54 (2020) 3064–3081.
[40] S. Indrawirawan, H.Q. Sun, X.G. Duan, S.B. Wang, J. Mater. Chem. A 3 (2015) 3432–3440.
[41] G. Liu, H. Lv, H. Sun, X. Zhou, Ind. Eng. Chem. Res. 57 (2018) 2396–2403.
[42] Y.N. Zhang, J. Wang, J. Chen, C. Zhou, Q. Xie, Environ. Sci. Technol. 52 (2018) 10490–10499.
[43] W. Ren, P. Zhou, G. Nie, et al., Water Res. 186 (2020) 116361.
[44] P. Hu, H. Su, Z. Chen, et al., Environ. Sci. Technol. 51 (2017) 11288–11296.
[45] T. Zhang, Y. Chen, Y. Wang, et al., Environ. Sci. Technol. 48 (2014) 5868–5875.
[46] X. Cheng, H. Guo, Y. Zhang, X. Wu, Y. Liu, Water Res. 113 (2017) 80–88.
[47] J. Lee, S. Hong, Y. Mackeyev, et al., Environ. Sci. Technol. 45 (2011) 10598–10604.
[48] Y. Jia, L. Zhang, A. Du, et al., Adv. Mater. 28 (2016) 9532–9538.
[49] Y. Gao, Z. Chen, Y. Zhu, T. Li, C. Hu, Environ. Sci. Technol. 54 (2020) 1232–1241.
[50] J. Kim, T. Zhang, W. Liu, et al., Environ. Sci. Technol. 53 (2019) 13312–13322.
[51] H. Ji, W. Liu, F. Sun, et al., Chem. Eng. J. 419 (2021) 129605.
[52] C. Dang, F. Sun, H. Jiang, et al., J. Hazard. Mater. 400 (2020) 123225.